Bulk spin torque driven perpendicular magnetization switching in L1 0 FePt

Meng Tang, Ka Shen, Shijie Xu, Huanglin Yang, Shuai Hu, Weiming Lü, Changjian Li, Mengsha Li, Zhe Yuan, Stephen Pennycook, et al.

Bulk spin torque driven perpendicular magnetization switching in $L1_0$ FePt

Meng Tang[1], Ka Shen[2], Shijie Xu[1], Huanglin Yang[1], Shuai Hu[1], Weiming Lü[3,4], Changjian Li[5], Mengsha Li[5], Zhe Yuan[2], Stephen Pennycook[5], Ke Xia[2], Aurelien Manchon[6*], Shiming Zhou[1], Xuepeng Qiu[1*]

[1]*Shanghai Key Laboratory of Special Artificial Microstructure Materials and Technology & School of Physics Science and Engineering, Tongji University, Shanghai 200092, China*

[2]*Department of Physics, Beijing Normal University, Beijing 100875, China*

[3]*Spintronics Institute, University of Jinan, Jinan 250022, China*

[4]*Condensed Matter Science and Technology Institute, School of Science, Harbin Institute of Technology, Harbin 150081, China*

[5]*Department of Materials Science and Engineering, National University of Singapore, 117576, Singapore*

[6]*Division of Physical Science and Engineering, King Abdullah University of Science and Technology (KAUST), Thuwal 23955, Saudi Arabia*

*e-mail: aurelien.manchon@kaust.edu.sa; xpqiu@tongji.edu.cn

Modern information technology demands advanced storage material and efficient data writing scheme. Inherent with a superior perpendicular magnetocrystalline anisotropy, the FePt in $L1_0$ phase envisions magnetic storage with ultrahigh capacity. However, reversing FePt magnetic state and therefore the encoded information has been proven to be extremely difficult. Here, we demonstrate that an electric current is capable to exert a large spin torque on a $L1_0$ FePt magnet, which ultimately leads to reversible magnetization switching through domain nucleation and expansion in an efficient and simple manner.

The spin torque effect increases with FePt thickness, exhibiting a bulk characteristic. Meanwhile, the spin torque effective fields and switching efficiency are found to increase when FePt approaches larger chemical ordering with higher crystallinity and stronger spin-orbit strength. Nontrivial gradients of lattice constant and chemical order are identified in the film normal direction, which serve as the symmetry breaking to generate spin torque of $L1_0$ FePt as further supported by quantum transport calculations. By exploring spin torque that survives in the volume of highly ordered ferromagnetic alloys, our results not only push forward the frontier of the material systems for generating spin torque, but also bring a transformative impact to the magnetic storage and spin memory applications with simple architecture, ultra-high density and readily application.

The demand for energy-efficient and high-density information storage has explosively increased during the past half-century, which has been carried forward by the advances of magnetic materials as the mainstay of storage media. One of the most transformative tendency of magnetic storage is to use a materials with high perpendicular magnetic anisotropy thereby allowing stable information retention in reduced magnet size, *i.e.*, elevated storage density[1]. The FePt in $L1_0$ phase possesses one of the highest perpendicular magnetocrystalline anisotropy among transition metal compounds. Along with its strong magnetization, $L1_0$ FePt is superior for vast information applications such as HDD (hard disk drive), MRAM (magnetic random access memory) and spin logic circuit. However, reversing the magnetization of $L1_0$ FePt is extremely challenging. Although different strategies such as HAMR (heat assisted magnetic recording)[2], MAMR (microwave assisted magnetic recording)[3] or external voltage control[4] *etc*. have been proposed to ease the magnetization switching of $L1_0$ FePt, major issues such as reliability,

compatibility or efficiency still inhibit them from practical applications. Therefore, a simple and efficient means to reorient the magnetization of $L1_0$ FePt is highly desirable for further advancing modern information technologies.

The origins of the high magnetic anisotropy of $L1_0$ FePt lie in the strong coupling between spin and orbital angular momenta and hybridization between Pt 5*d* and Fe 3*d* electrons[5-7]. The former, *i.e.*, the spin-orbit coupling (SOC), is also the premise of recently emerging spin-orbit torque (SOT) effect[8-11], thereby opening new avenues for the possible electrical manipulation of magnetization for $L1_0$ FePt[12, 13]. However, the emergence of SOT has hitherto been associated with the inversion symmetry breaking that happens either at normal metal/ferromagnet interface or inside the bulk ferromagnet structure[9, 10, 14, 15]. In contrast, $L1_0$ FePt is a centrosymmetric alloy without symmetry breaking for either the global crystal or specific atomic site and therefore the electric current induced spin polarization tends to vanish in $L1_0$ FePt from the perspective of crystalline symmetry. Although inversion symmetry breaking is a crucial ingredient to obtain overall non-vanishing spin-orbit torques[11], recent studies have implied the possibility of generating spin-orbit mediated torque in ferromagnets with centrosymmetric crystalline structure or alternative stacking layers structure[16, 17]. In the former[16], the spin accumulation arising at the edges of the sample can be engineering to obtain current-driven domain nucleation, while in the latter[17], local lattice mismatch leads to local spin-orbit torque with bulk-like characteristics.

Here, we demonstrate the current induced magnetization switching in the *single* $L1_0$ FePt layers. Despite the large perpendicular anisotropy field that approaches several Tesla, the magnetization of $L1_0$ FePt can be reversibly switched between up and down states as characterized by anomalous Hall effect measurements and polar Kerr microscopy. The

magnetization reverses through domain nucleation and expansion. The current induced magnetization switching efficiency as well as the quantified effective magnetic fields is found to *increase* with film thickness. Remarkably, the spin torque effect in $L1_0$ FePt increases with the crystallinity and spin-orbit coupling, and its emergence is found to be driven by a structural gradient in the film volume. This discovery opens a new paradigm for generating spin-orbit mediated torque in single ferromagnetic alloy with great prospects such as simple structure, ultra-high density and readily application.

Results

Structural and magnetic properties. The $L1_0$ FePt is a face-centered tetragonal magnetic alloy with alternating Pt and Fe atomic layers as schematically shown in Figure 1a. Using high temperature deposition and subsequent annealing, highly ordered $L1_0$ FePt has been successfully grown on (001) MgO single-crystal substrate. Figure 1b shows the x-ray diffraction (XRD) spectra for a 12 nm FePt and the MgO substrate. The chemical ordering degree S is derived from the intensity of the (001) and (002) peaks[6]. The large S of 0.96, together with the pole figure of FePt (111) diffraction peak (Supplementary Information S1), demonstrates the epitaxial growth of high quality $L1_0$ FePt on MgO single-crystal substrate. Figure 1c shows the in-plane and out-of-plane magnetic hysteresis loops for the 12 nm FePt. The sample exhibits a saturation magnetization M_S=1000 emu/cc and a large in-plane saturation field around 7.4 Tesla that affirming the strong perpendicular magnetic anisotropy. In addition, high resolution cross-section scanning transmission electron microscopy (STEM) and electron energy loss spectroscopy (EELS) were performed (Fig. 1d). While a small amount of Pt (~2 atomic layers) segregates at the top surface of FePt, highly ordered alternative stacking of Fe and Pt atomic layers can be clearly resolved from the high-angle annular dark field (HAADF) image, which is further

supported by the elementary analysis of Pt and Fe from EELS elemental mapping result for the region of red square in Fig. 1d.

Current induced magnetization switching. The magnetization switching is performed with in-plane pulsed current injection as schematically shown in Figure 2a. Pulsed currents (pulse width of 200 μs) with varied amplitude are applied to the 10 μm Hall bar device of 4 nm $L1_0$ FePt. After application of each current pulse, the Hall resistance and polar Kerr image are simultaneously recorded. It should be noted that the Hall resistance is measured with a small pulsed current (with a current density of ~10^5 A/cm^2), thus the equilibrium magnetization direction can be recorded without disturbances from current induced spin torque and Joule heating. Both the anomalous Hall resistance R_H and polar Kerr signal probe the average *z*-component of the FePt magnetization, thereby allowing the observation of perpendicular magnetization switching.

Figure 2b shows the R_H as a function of the pulsed current. As can be seen, reversible current induced magnetization switching is achieved with an external magnetic field along x axis (H_x=±1.2 kOe) while no hysteresis switching is observed for H_x=0 Oe and H_y=1.2 kOe. Opposite switching polarities are observed when reversing H_x. These switching features are similar to the SOT switching in perpendicular magnetized normal metal/ferromagnet heterostructures[9, 10], suggesting the similarity of underlying driving torque. The magnetization switching process is simultaneously recorded and visualized by the polar magneto-optical Kerr effect (MOKE) microscopy, and the corresponding Kerr images of the states marked in Fig. 2b are shown in Fig. 2c. As the bright and dark contrasts in the Kerr images scale with the up and down components of magnetization, respectively, the consecutive changes of Kerr contrast in Fig. 2c confirm the perpendicular magnetization switching in the FePt device. Moreover, the Kerr images of the

states 2 and 4 both show the magnetic domain formation during the reversal process. The application of electric current triggers the domain wall nucleation and expansion, leading to reversible magnetization switching.

Bulk characteristics of spin torque effect. The current induced magnetization switching and harmonic Hall voltage measurements are performed for $L1_0$ FePt with varied thickness t = 4, 8, 12, 16 and 20 nm. The sample properties are characterized and shown in Supplementary Information S1. Here, the harmonic Hall voltage measurements are utilized to quantitatively characterize the current induced effective magnetic fields[18, 19]. Figure 3a-d show the harmonic measurement results for the two measurement schemes, namely the longitudinal and transverse measurement schemes. In the longitudinal (transverse) scheme, the in-plane magnetic field is swept along (transverse to) the current direction, allowing the longitudinal (transverse) effective magnetic field H_L (H_T) of the current induced spin torques to be characterized separately. The planar Hall effect is considered in the analysis to address the entanglement between H_L and H_T. In addition, the anomalous Nernst effect originating from the in-plane and out-of-plane temperature gradients is found to be significant especially for the longitudinal scheme as seen from Fig. 3a (also in Supplementary Information S3). With consideration of both planar Hall and anomalous Nernst effects, the below equations are utilized to calculate current induced effective magnetic field H_L and H_T[19]:

$$H_L = -2\frac{B_x \pm 2\xi B_y}{1-4\xi^2} \tag{1}$$

$$H_T = -2\frac{B_y \pm 2\xi B_x}{1-4\xi^2} \tag{2}$$

where $B_x \equiv \frac{\partial V_{2f,//}}{\partial H} \Big/ \frac{\partial^2 V_f}{\partial H^2}$ and $B_y \equiv \frac{\partial V_{2f,\perp}}{\partial H} \Big/ \frac{\partial^2 V_f}{\partial H^2}$. ξ is the ratio between the planar and anomalous Hall resistances and ± denotes the magnetization direction that points either along +z or –z. Figure 3b and d show the thickness dependences of H_L and H_T. H_T is found to be larger than H_L by more than two times. Most remarkably and quite surprisingly, both H_L and H_T increase with t, in sharp contrast with the 1/t dependence expected for interfacial torques. This thickness dependence is neither explained by change in M_S, that remains mostly constant over the thickness range (see Supplementary Information S1), nor by modification of the sample conductivity. This increase of spin torque with thickness is further confirmed by the linear increase in the current induced magnetization switching efficiency, which is defined as $\eta = H_K / J_S$, with t as shown in Fig. 3e-f.

To gain further insight into the spin torque effect, the correlation between the bulk crystallinity and the spin torque effect in $L1_0$ FePt is studied. Here, the crystallinity of $L1_0$ FePt refers to the fraction of Fe (Pt) sites occupied by the Fe (Pt) atoms, which is in turn determined by the chemical ordering parameter (S) of the alloy and the alloy composition (x)[20]. To achieve ideal crystallinity of $L1_0$ FePt, one can enlarge the value of S and tune the alloy toward the stoichiometric $L1_0$ phase composition (x=0.5). The higher crystallinity of $L1_0$ alloy not only contributes to a larger perpendicular magnetocrystalline anisotropy but is also suggested to accommodate stronger spin-orbit coupling strength[21-24]. Here, we have modified the crystallinity of $L1_0$ FePt using two approaches: either by modifying the FePt composition or by changing the annealing temperature. The results of the former approach are shown in Figure 4a. By changing x of $Fe_{1-x}Pt_x$, the chemical ordering degree S is continuously tuned, and the maximal S emerges around x=0.51 (Supplementary Information S4). Furthermore, the derived H_L and H_T from

harmonic Hall voltage measurements as well as the switching efficiency also exhibit strong correlation with x. The coincidence of maximal values at x=0.51 for H_L, H_T, η and S suggests the spin torque effect in $L1_0$ FePt arises from crystallinity and spin-orbit coupling related mechanism.

Alternatively, we have examined the spin torque effect in $L1_0$ FePt with different annealing temperature T_A. While increasing T_A from 550 °C to 760 °C, the chemical ordering parameter S is tuned from 0.57 to 0.96 (Supplementary Information S5). Subsequent measurements demonstrate that H_L, H_T and η increase more than three times upon S optimization, as shown in Figure 4b. Therefore, both studies in Fig. 4 suggest the primary importance of crystallinity and of spin-orbit strength in the onset of the spin torque effect in $L1_0$ FePt.

Bulk structural gradient induced spin torque. The emergence of spin-orbit mediated torque and its driven magnetization switching in $L1_0$ FePt are counter-intuitive from the established framework of SOT. The only few examples of single ferromagnet possessing non-trivial spin torque are (Ga,Mn)As and NiMnSb[8, 14, 25]. However, all these ferromagnets lack inversion symmetry unlike the bulk $L1_0$ FePt which is centrosymmetric in the crystalline structure. Other elements of symmetry breaking, such as antiphase boundary, current induced temperature gradient and the surface Pt segregation have been observed in the sample. The antiphase boundary can break the inversion symmetry of FePt crystalline structure locally and hence promotes current-driven spin density. However, such an effect is difficult to correlate with the present results as it depends on the orientation of the boundary, which appears to be random across the FePt crystal as shown in the TEM images (Supplementary Information S7). Moreover, no explicit correlation between the anomalous Nernst effect and spin torque effect has been

found in the FePt thickness study, suggesting the minor role of temperature gradient in the spin torque effect (Supplementary Information S8). At last, the SOT generated by segregated Pt at surface is found to be negligible (Supplementary Information S9) and not in accordance with the *t*-scaling characteristic as in Fig. 3, thus it is also excluded to account for current experimental findings.

One possible symmetry breaking remaining to be considered is the gradient of the crystalline structure that manifests as the spatial evolutions of lattice constant and long range chemical ordering. This effect has been found in thin films of crystal due to the strain relaxation [17, 26-28]. To test this hypothesis, we examine the depth profile of FePt crystalline structure by a combined technique of ion milling and XRD measurements (Supplementary Information S6). Sequential ion millings are utilized to reach different depth of a 24 nm $L1_0$ FePt film, and the XRD measurement is performed after each milling to acquire *c* and *S* with ultrafine resolution [29-31]. Indeed, as shown in Fig. 5a, both *c* and *S* are observed to vary continuously along the thickness direction. As *c* and *S* are independently determined by the position and the intensity of XRD peaks, respectively, the similar variation trends of their depth profiles affirm the chemical disorder gradient along the film depth *i.e.*, the change of occupation fraction of Fe (Pt) atoms in their designated sites. *c* approximately decreases from the bottom MgO/FePt interface to the top film surface. More remarkably, *S* shows significant spatial variation that changes from 0.48 ± 0.12 to 0.96 ± 0.02 as show in Fig. 5a. With such chemical gradient, the symmetry of crystalline structure in FePt breaks, which can produce a sizable torque throughout the thickness of the FePt slab.

The pertinence of above idea has been tested by building a ferromagnetic slab within the tight-binding approximation and by computing the current-driven torque using Kubo formula.

Here, in the absence of handbook parameters for $L1_0$ FePt, a slab of bcc Fe(001) for a thickness of 20 ML ($\approx 5.6\,nm$) has been considered using Slater-Koster parametrization[32]. A gradient of disorder throughout the slab's thickness *t* has been modeled with a homogeneous broadening of random potential $\Gamma(t)$. More details of the calculation can be found in the Supplementary Information S10. Figure 5b shows the torque obtained as a function of the gradient of disorder $\delta\Gamma$, for an average disorder strength $\Gamma_0 = 13$ meV, which corresponds to the "ideal" conductivity of bcc Fe, $\sigma_{Fe} = 10^7\Omega^{-1} \cdot m^{-1}$. As can be seen, when both torque components are zero without $\delta\Gamma$, they increase linearly as a function of the disorder gradient, thus indicating that a reasonable gradient of disorder can maintain a sizable torque throughout the volume of an otherwise centrosymmetric ferromagnet. On the other hand, by accounting for the experimental fact that the gradient of disorder is accompanied by a gradient of chemical ordering *S*, the thickness dependence of SOT can be readily understood by the proportional correlation between *t* and *S* (and thus the SOC strength) which ultimately leads to the *t*-scaling characteristic of SOT.

While we have elucidated the spin torque effect in $L1_0$ FePt to a certain extent, the full understanding and the establishment of complete physical picture still wait for more research works. Especially, the derived effective magnetic fields appear too small to adequately account for the magnetization switching of $L1_0$ FePt that possesses extraordinarily large perpendicular anisotropy. Such a discrepancy can be ascribed to the fact that the effective fields are derived for the magnetic saturation states, while the current induced magnetization switching is achieved through the domain nucleation and expansion processes. Therefore, conventional spin transfer torque may emerge for the $L1_0$ FePt with multi-domains[33, 34]. On the other hand, the SOT is believed to be magnetization dependent[18, 35, 36], possibly leading to significantly augmented SOT inside magnetic domain wall with evolutive magnetization direction.

At last, it is noted that the conventional SOT originating from the symmetry breaking places strong restrictions to the material parameters and device architecture. For example, the interfacial nature of SOT in normal metal/ferromagnet heterostructures maximizes the torque strength only for a very thin ferromagnet which shrinks the thermal stability and the nonvolatility[10]. Moreover, the conventional SOT devices mostly require 3 terminals architecture thereby significantly increasing the device complexity[37, 38]. The bulk spin torque observed in the centrosymmetric $L1_0$ FePt shows a potential to remove these fundamental obstacles and brings new perspectives for SOT research and applications.

Methods

Sample preparations and characterization.

FePt films were deposited onto MgO (001) substrates by high vacuum magnetron sputtering at an elevated temperature, and a 2 hours *in-situ* annealing was subsequently followed at the same temperature to promote the formation of $L1_0$ phase of FePt alloy. For films of varying thickness and varying composition, the temperature for both the deposition and annealing was slightly adjusted in the range from 600 to 760 °C for each film to obtain a high-intensity FePt (001) diffraction peak and a good perpendicular magnetic anisotropy. A Fe target with several small Pt slices on its surface was used to simultaneously sputter Pt and Fe atoms. The composition of $Fe_{1-x}Pt_x$ samples was varied by changing the number of Pt slices. The thickness and crystal structure were characterized by X-ray reflection (XRR) and X-ray diffraction (XRD) techniques with a Bruker D8 Discover diffractometer using Cu Kα radiation (λ=0.15419 nm). The composition of the films was analyzed by Energy Dispersive X-ray Spectroscopy (EDS) with an Oxford X-max^{80} scanning electron microscope (SEM). The magnetic properties of the films were measured by a vibrating sample magnetometer (VSM) module of a Physical Property Measurement System (PPMS) or a Lakeshore VSM. The FePt Hall bar devices, with a width of 10 μm, were prepared by ultra-violet lithography and Ar ion milling.

Magnetization switching measurements.

The current driven magnetization switching was detected both by electrical measurement and MOKE at room temperature. A combination of Keithley 6221 source-meter and 2182A nanovoltmeter was utilized for the electrical measurements. The simultaneous detection of Hall signal and MOKE signal was carried out in an optical platform equipped with a polar Kerr microscope using LED as light source (Tuotuo technology). For each step in a R_H-I loop a dc

current pulse of amplitude I with duration of 200 μs was applied to the Hall bar device as write current, 6 seconds later a probe current pulse of 0.5 mA with duration of 2 ms was applied and the Hall voltage was measured with a 1ms delay by 2182A. The write current was varied to obtain a complete R_H-I loop. The electrical detection of Hall signal for current induced magnetization switching was also implemented in PPMS without acquiring MOKE images.

Harmonic Hall voltage measurements.

The devices were first magnetized to a saturated state by applying a large field (±1.6 T) perpendicular to the film plane. A sinusoidal ac current of 13.7 Hz was applied by Keithley 6221 source-meter and the first and second harmonic Hall voltages were simultaneously measured by two Stanford SR830 lock-in amplifiers during sweeping an in-plane field along (H_x) or transverse (H_y) to current direction. The amplitude of the sinusoidal current varies as the thickness of FePt to keep a constant current density of 1×10^7 A/cm^2.

STEM measurements.

High-resolution STEM-high angle annular dark field (STEM-HAADF) imaging were performed using the JEOL-ARM200F microscope equipped with ASCOR aberration corrector and cold-field emission gun and operated at 200 kV. The cross-section TEM samples were prepared by a focused ion beam (FIB) machine (FEI Versa 3D) with 30 kV Ga ions, followed by a 2 kV low voltage cleaning step. The HAADF images were acquired with probe forming angle 30 mrad and collection angle of 68-280 mrad. EELS elemental mapping was recorded using a Gatan Quantum ER spectrometer with a 1 eV/channel energy dispersion.

Data availability.

The data that support the findings of this study are available from the corresponding author on reasonable request.

References

[1] S. Iwasaki, Perpendicular magnetic recording-Its development and realization, Journal of Magnetism and Magnetic Materials **324,** 244-247 (2012).
[2] T. Seki, K. Utsumiya, Y. Nozaki, H. Imamura, K. Takanashi, Spin wave-assisted reduction in switching field of highly coercive iron-platinum magnets, Nature Communications **4,** 1726 (2013).
[3] W.A. Challener, C. Peng, A.V. Itagi, D. Karns, W. Peng, Y. Peng, X. Yang, X. Zhu, N.J. Gokemeijer, Y.T. Hsia, G. Ju, R.E. Rottmayer, M.A. Seigler, E.C. Gage, Heat-assisted magnetic recording by a near-field transducer with efficient optical energy transfer, Nature Photonics **3,** 220-224 (2009).
[4] M. Weisheit, S. Fähler, A. Marty, Y. Souche, C. Poinsignon, D. Givord, Electric Field-Induced Modification of Magnetism in Thin-Film Ferromagnets, Science **315,** 349-351 (2007).
[5] K.M. Seemann, Y. Mokrousov, A. Aziz, J. Miguel, F. Kronast, W. Kuch, M.G. Blamire, A.T. Hindmarch, B.J. Hickey, I. Souza, C.H. Marrows, Spin-Orbit Strength Driven Crossover between Intrinsic and Extrinsic Mechanisms of the Anomalous Hall Effect in the Epitaxial $L1_0$-Ordered Ferromagnets FePd and FePt, Physical Review Letters **104,** 076402 (2010).
[6] P. He, L. Ma, Z. Shi, G.Y. Guo, J.G. Zheng, Y. Xin, S.M. Zhou, Chemical Composition Tuning of the Anomalous Hall Effect in Isoelectronic $L1_0$ $FePd_{1-x}Pt_x$ Alloy Films, Physical Review Letters **109,** 066402 (2012).
[7] S. Miwa, M. Suzuki, M. Tsujikawa, K. Matsuda, T. Nozaki, K. Tanaka, T. Tsukahara, K. Nawaoka, M. Goto, Y. Kotani, T. Ohkubo, F. Bonell, E. Tamura, K. Hono, T. Nakamura, M. Shirai, S. Yuasa, Y. Suzuki, Voltage controlled interfacial magnetism through platinum orbits, Nature Communications **8,** 15848 (2017).
[8] A. Chernyshov, M. Overby, X. Liu, J.K. Furdyna, Y. Lyanda-Geller, L.P. Rokhinson, Evidence for reversible control of magnetization in a ferromagnetic material by means of spin–orbit magnetic field, Nature Physics **5,** 656-659 (2009).
[9] I.M. Miron, K. Garello, G. Gaudin, P.-J. Zermatten, M.V. Costache, S. Auffret, S. Bandiera, B. Rodmacq, A. Schuhl, P. Gambardella, Perpendicular switching of a single ferromagnetic layer induced by in-plane current injection, Nature **476,** 189-193 (2011).
[10] X. Qiu, Z. Shi, W. Fan, S. Zhou, H. Yang, Characterization and Manipulation of Spin Orbit Torque in Magnetic Heterostructures, Advanced Materials **30,** 1705699 (2018).
[11] A. Manchon, J. Zelezny, I.M. Miron, T. Jungwirth, J. Sinova, A. Thiaville, K. Garello, P. Gambardella, Current-induced spin-orbit torques in ferromagnetic and antiferromagnetic systems, arXiv:1801.09636 DOI (2019).
[12] B. Zimmermann, N.H. Long, P. Mavropoulos, S. Blügel, Y. Mokrousov, Influence of complex disorder on skew-scattering Hall effects in $L1_0$-ordered FePt alloy, Physical Review B **94,** 060406(R) (2016).
[13] G. Géranton, B. Zimmermann, N.H. Long, P. Mavropoulos, S. Blügel, F. Freimuth, Y. Mokrousov, Spin-orbit torques and spin accumulation in FePt/Pt and Co/Cu thin films from first principles: The role of impurities, Physical Review B **93,** 224420 (2016).
[14] C. Ciccarelli, L. Anderson, V. Tshitoyan, A.J. Ferguson, F. Gerhard, C. Gould, L.W. Molenkamp, J. Gayles, J. Železný, L. Šmejkal, Z. Yuan, J. Sinova, F. Freimuth, T. Jungwirth, Room-temperature spin–orbit torque in NiMnSb, Nature Physics **12,** 855-860 (2016).
[15] X. Zhang, Q. Liu, J.-W. Luo, A.J. Freeman, A. Zunger, Hidden spin polarization in inversion-symmetric bulk crystals, Nature Physics **10,** 387-393 (2014).
[16] C.O. Pauyac, M. Chshiev, A. Manchon, S.A. Nikolaev, Spin Hall and Spin Swapping Torques in Diffusive Ferromagnets, Physical Review Letters **120,** 176802 (2018).
[17] M. Jamali, K. Narayanapillai, X. Qiu, L.M. Loong, A. Manchon, H. Yang, Spin-Orbit Torques in Co/Pd Multilayer Nanowires, Physical Review Letters **111,** 246602 (2013).

[18] X. Qiu, P. Deorani, K. Narayanapillai, K.-S. Lee, K.-J. Lee, H.-W. Lee, H. Yang, Angular and temperature dependence of current induced spin-orbit effective fields in Ta/CoFeB/MgO nanowires, Scientific Reports **4,** 4491 (2014).
[19] M. Hayashi, J. Kim, M. Yamanouchi, H. Ohno, Quantitative characterization of the spin-orbit torque using harmonic Hall voltage measurements, Physical Review B **89,** 144425 (2014).
[20] B.E. Warren, X-ray Diffraction, Dover Publications, Inc., New York, 1990.
[21] M. Chen, Z. Shi, W.J. Xu, X.X. Zhang, J. Du, S.M. Zhou, Tuning anomalous Hall conductivity in $L1_0$ FePt films by long range chemical ordering, Applied Physics Letters **98,** 082503 (2011).
[22] L.J. Zhu, D. Pan, J.H. Zhao, Anomalous Hall effect in epitaxial $L1_0$-$Mn_{1.5}Ga$ films with variable chemical ordering, Physical Review B **89,** 220406(R) (2014).
[23] W.J. Fan, Z. Shi, F.L. Chen, S.M. Zhou, Tuning Effects of Spin–Orbit Coupling in $L1_0$ Ordered and Disordered FePdPt Films, SPIN **5,** 1530004 (2015).
[24] T. Seki, K.-i. Uchida, T. Kikkawa, Z. Qiu, E. Saitoh, K. Takanashi, Observation of inverse spin Hall effect in ferromagnetic FePt alloys using spin Seebeck effect, Applied Physics Letters **107,** 092401 (2015).
[25] H. Kurebayashi, J. Sinova, D. Fang, A.C. Irvine, T.D. Skinner, J. Wunderlich, V. Novák, R.P. Campion, B.L. Gallagher, E.K. Vehstedt, L.P. Zârbo, K. Výborný, A.J. Ferguson, T. Jungwirth, An antidamping spin–orbit torque originating from the Berry curvature, Nature Nanotechnology **9,** 211-217 (2014).
[26] A. Zhang, X. Wu, S. Tang, S. Zhou, Enhancement of magnetic anisotropy for $L1_0$-(0 0 1) FePt films grown on $SrTiO_3$ substrate, Chemical Physics Letters **654,** 135-138 (2016).
[27] J. Lucy, A. Hauser, Y. Liu, H. Zhou, Y. Choi, D. Haskel, S.G. Te Velthuis, F. Yang, Depth-resolved magnetic and structural analysis of relaxing epitaxial Sr 2 CrReO 6, Physical Review B **91,** 094413 (2015).
[28] C. Burrows, T. A. Hase, M. Ashwin, P. Mousley, G. Bell, Depth sensitive X-ray diffraction as a probe of buried half-metallic inclusions, physica status solidi (b) **254,** 1600543 (2017).
[29] M. Ahart, M. Somayazulu, R. Cohen, P. Ganesh, P. Dera, H.-k. Mao, R.J. Hemley, Y. Ren, P. Liermann, Z. Wu, Origin of morphotropic phase boundaries in ferroelectrics, Nature **451,** 545 (2008).
[30] Z. Huang, M. Bartels, R. Xu, M. Osterhoff, S. Kalbfleisch, M. Sprung, A. Suzuki, Y. Takahashi, T.N. Blanton, T. Salditt, Grain rotation and lattice deformation during photoinduced chemical reactions revealed by in situ X-ray nanodiffraction, Nature Materials **14,** 691 (2015).
[31] Y.-Z. Zheng, Y.-L. Soo, S.-L. Chang, Depth profiles of the interfacial strains of Si 0.7 Ge 0.3/Si using three-beam Bragg-surface diffraction, Scientific Reports **6,** 25580 (2016).
[32] J.C. Slater, G.F. Koster, Simplified LCAO method for the periodic potential problem, Physical Review **94,** 1498 (1954).
[33] D.C. Ralph, M.D. Stiles, Spin transfer torques, Journal of Magnetism and Magnetic Materials **320,** 1190-1216 (2008).
[34] G. Tatara, H. Kohno, Theory of current-driven domain wall motion: Spin transfer versus momentum transfer, Physical Review Letters **92,** 086601 (2004).
[35] C. Ortiz Pauyac, X. Wang, M. Chshiev, A. Manchon, Angular dependence and symmetry of Rashba spin torque in ferromagnetic heterostructures, Applied Physics Letters **102,** 252403 (2013).
[36] K.-S. Lee, D. Go, A. Manchon, P.M. Haney, M.D. Stiles, H.-W. Lee, K.-J. Lee, Angular dependence of spin-orbit spin-transfer torques, Physical Review B **91,** 144401 (2015).
[37] M. Cubukcu, O. Boulle, M. Drouard, K. Garello, C. Onur Avci, I. Mihai Miron, J. Langer, B. Ocker, P. Gambardella, G. Gaudin, Spin-orbit torque magnetization switching of a three-terminal perpendicular magnetic tunnel junction, Applied Physics Letters **104,** 042406 (2014).
[38] S.W. Lee, K.J. Lee, Emerging Three-Terminal Magnetic Memory Devices, Proceedings of the IEEE **104,** 1831-1843 (2016).

Acknowledgements

This work was supported by the National Key R&D Program of China Grand No. 2015CB921501 and 2017YFA0305300, the National Science Foundation of China Grant Nos. 11674246, 51331004 and 51671147, Natural Science Foundation of Shanghai Grant No. 17ZR1443700, Shanghai Pujiang Program No. 16PJ1409300, the Program for Professor of Special Appointment (Eastern scholar) at Shanghai Institutions of Higher Learning No. TP2016016, and the Fundamental Research Funds for the Central Universities. A. M. was supported by the King Abdullah University of Science and Technology (KAUST).

Author contributions

M.T., S.Z. and X.Q. planned the project. M.T. and S.X. fabricated the samples. M.T. and H.Y. performed measurements. K.S., K.X. and A.M. provided the theory. All authors discussed the results and commented on the manuscript. M.T., A.M. and X.Q. wrote the manuscript. S.Z. and X.Q. initiated the idea and led the project.

Additional information

Competing financial interests: The authors declare no competing financial interests.

Correspondence and requests for materials should be addressed to A.M. (aurelien.manchon@kaust.edu.sa) and X.Q. (xpqiu@tongji.edu.cn)

Figure captions

Fig. 1. Crystal structure and magnetic property of $L1_0$ FePt. a, The crystallographic unit cell of $L1_0$ FePt. Fe atoms and the associated spins are depicted by the red spheres and arrows, Pt atoms are depicted by the blue spheres. **b**, θ - 2θ XRD spectra of the 12 nm FePt and the referenced (001) MgO substrate. **c**, In-plane (yellow) and out-of-plane (blue) magnetization curves for the 12 nm FePt. **d**, High-angle annular dark field (HAADF) and electron energy loss spectroscopy (EELS) images of the FePt sample. The corresponding EELS region is indicated in the red box in the HAADF image.

Fig. 2. Current induced magnetization switching in $L1_0$ FePt. a, Schematic for measurements of current induced magnetization switching that is simultaneously recorded by Hall voltage measurement and Kerr microscopy imaging. **b**, R_H versus pulsed DC current I. The assisted external magnetic field is indicated with each curve. **c,** Kerr images recorded for the states 1-5 as indicated in (**b**).

Fig. 3. Bulk spin torque scales with $L1_0$ FePt thickness. a-d, Quantification of the current induced effective magnetic fields by harmonic Hall voltage measurements. The first and second harmonic signals in fully saturated magnetic states (magnetization pointing long +Z or -Z are indicated by M↑ and M↓, respectively) were recorded with an in-plane magnetic field along (**a**) and transverse (**c**) to the current direction. In **a** and **c**, the solid and open symbols in V_{2f} curves correspond to the original measurement signal and the one with correction of anomalous Nernst effect respectively for a FePt sample with t=12 nm. The derived effective field, including both H_L (**b**) and H_T (**d**), versus FePt thickness t. **e-f**, Current induced magnetization switching (**e**) and the switching efficiency η_{SOT} (**f**) with different t.

Fig. 4. Correlation between spin orbit coupling and spin torque in FePt. a, H_L, H_T and η_{SOT} vs. x. **b**, H_L, H_T and η_{SOT} vs. annealing temperature T_A. The FePt thickness is fixed as 12 nm.

Fig. 5. Structural gradient induced spin torque. a, Depth profile of lattice constant c and order parameter S for a 24-nm-thick FePt film. The data were obtained by a combination technique of ion milling and XRD measurements (Supplementary Information S6). **b,** Calculations of longitudinal torque (τ_L, red line) and transverse torque (τ_T, blue line) as a function of parameter $\delta\Gamma$, gradient of disorder, for $\Gamma_0 = 13$ meV.

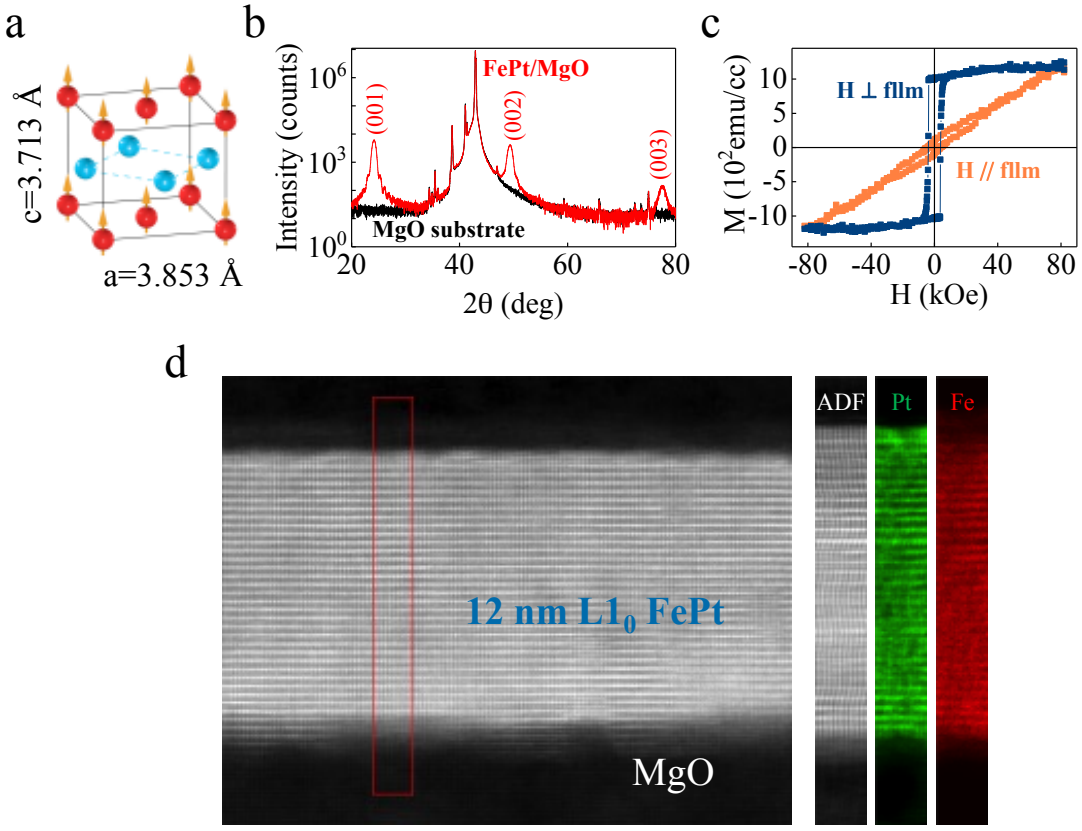
a
c=3.713 Å
a=3.853 Å
b
Intensity (counts)
FePt/MgO
(001)
(002)
(003)
MgO substrate
2θ (deg)
c
M (10²emu/cc)
H ⊥ fllm
H // fllm
H (kOe)
d
12 nm L1₀ FePt
MgO
ADF
Pt
Fe

Figure 1

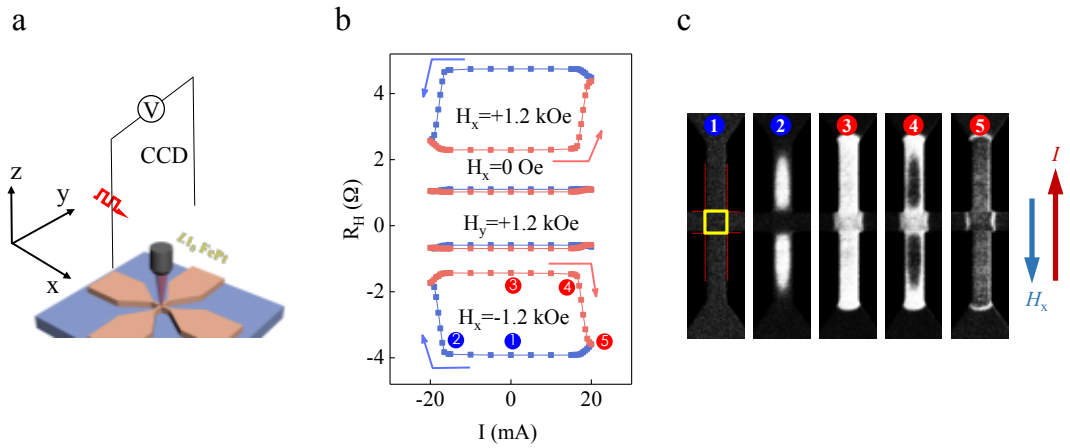
a
b
c
V
CCD
z
y
x
$L1_0$ FePt
H_x=+1.2 kOe
H_x=0 Oe
H_y=+1.2 kOe
H_x=-1.2 kOe
R_H (Ω)
I (mA)
4
2
0
-2
-4
-20
0
20
1
2
3
4
5
I
H_x

Figure 2

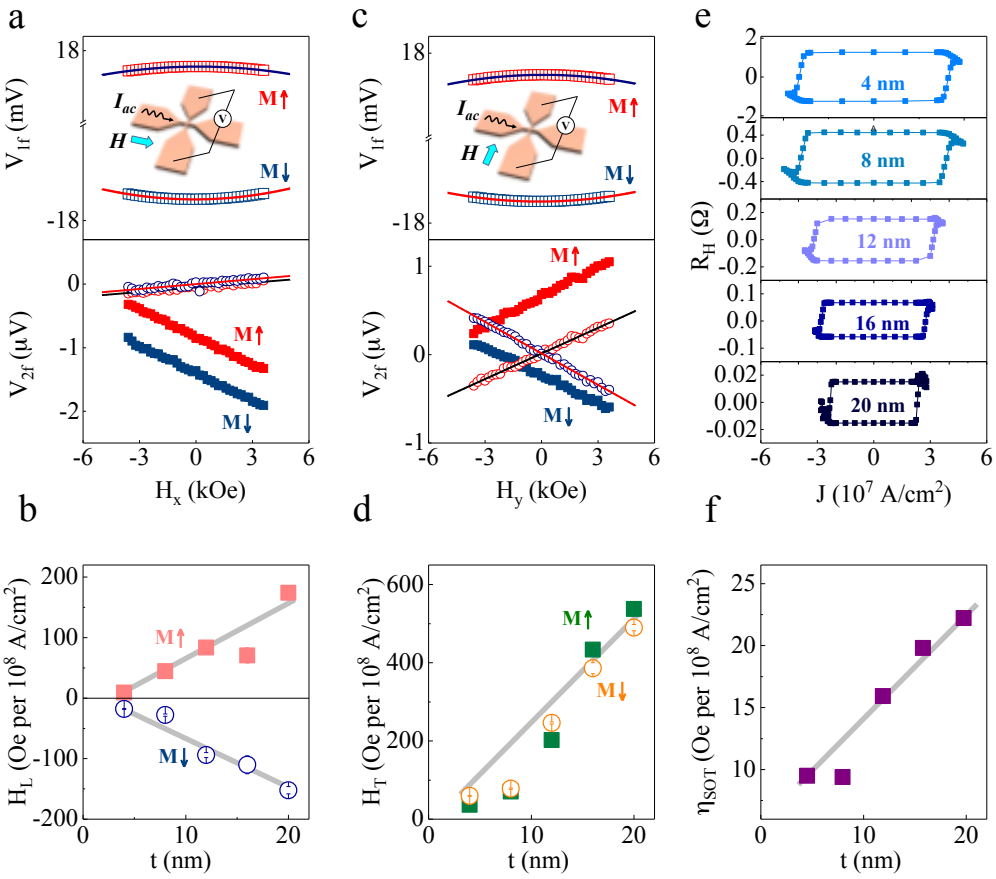
a
c
e
b
d
f
V_{1f} (mV)
V_{2f} (μV)
I_{ac}
H
M↑
M↓
V
H_x (kOe)
H_y (kOe)
R_H (Ω)
4 nm
8 nm
12 nm
16 nm
20 nm
J (10^7 A/cm^2)
H_L (Oe per 10^8 A/cm^2)
H_T (Oe per 10^8 A/cm^2)
η_{SOT} (Oe per 10^8 A/cm^2)
t (nm)

Figure 3

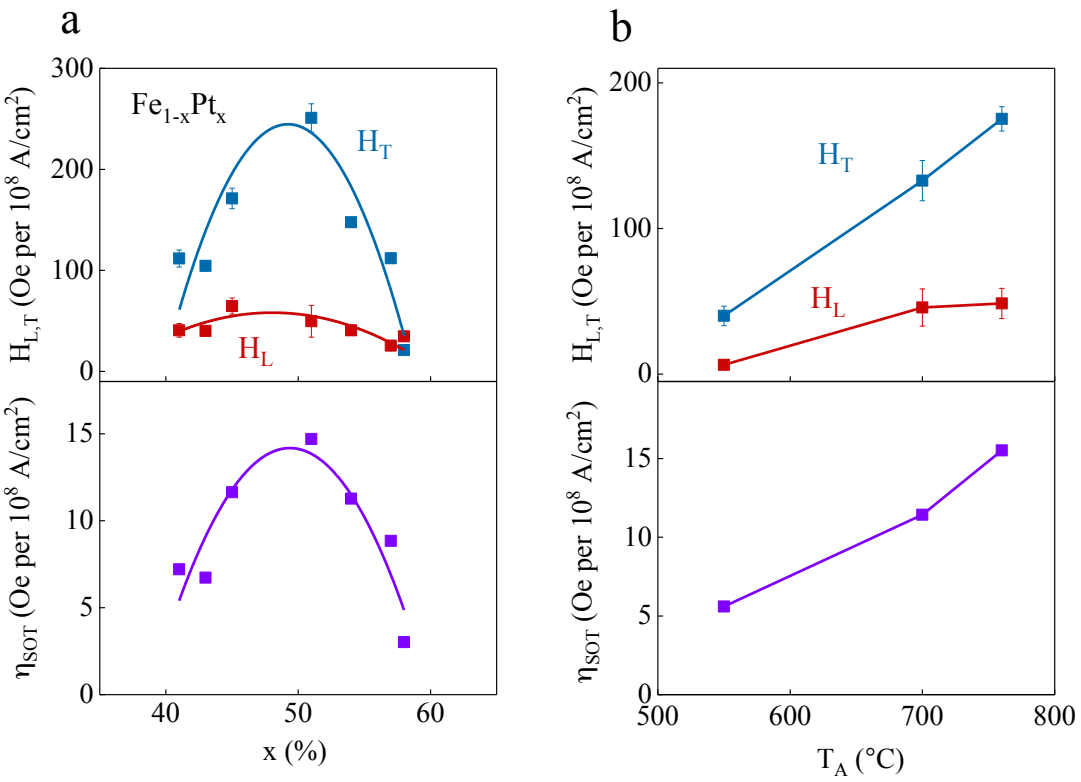
a
b
Fe1-xPtx
HT
HL
HL,T (Oe per 10^8 A/cm^2)
ηSOT (Oe per 10^8 A/cm^2)
x (%)
TA (°C)
300
200
100
0
15
10
5
40
50
60
500
600
700
800

Figure 4

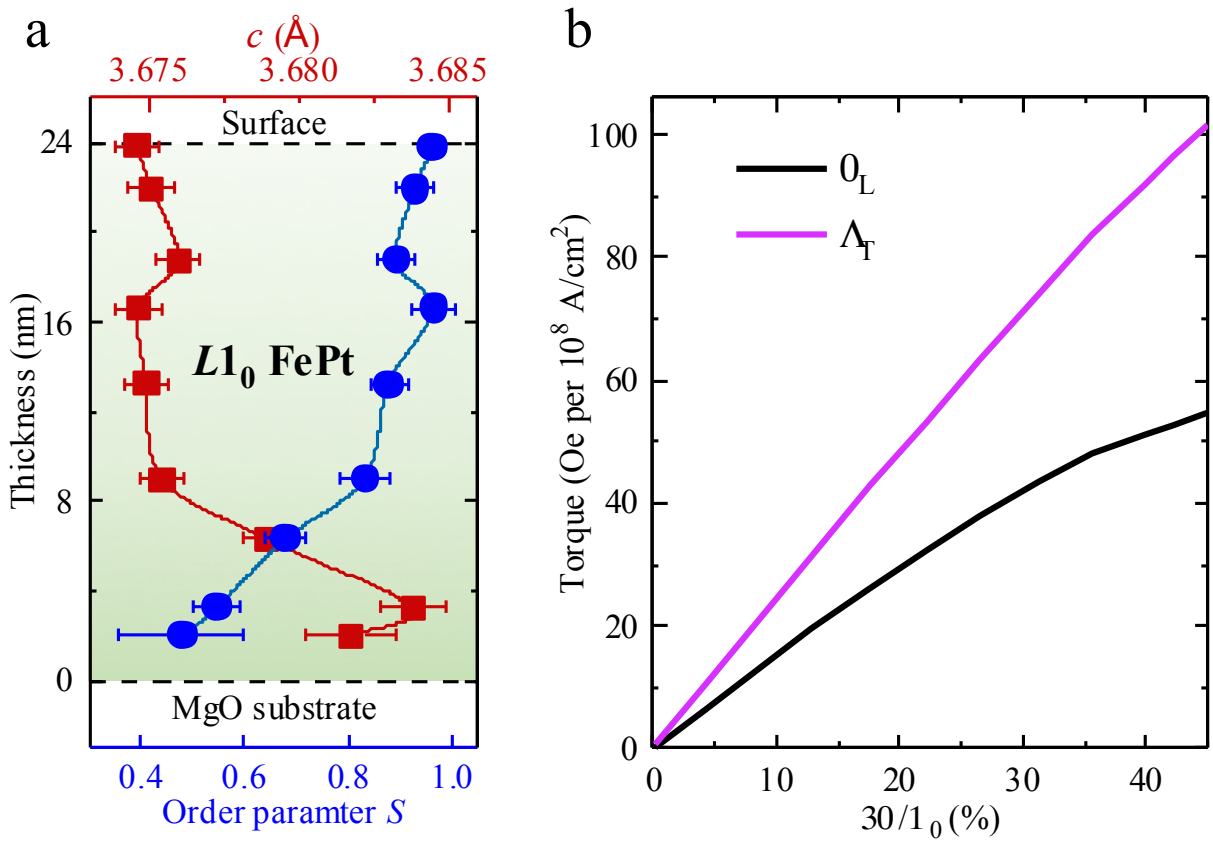
a
c (Å)
3.675
3.680
3.685
Surface
24
16
8
0
Thickness (nm)
L1₀ FePt
MgO substrate
0.4
0.6
0.8
1.0
Order paramter S
b
100
80
60
40
20
0
Torque (Oe per 10⁸ A/cm²)
0L
ΛT
0
10
20
30
40
30/10 (%)

Figure 5